HYDROGEN STORAGE IN CARBON NANOMATERIALS AT LOW TEMPERATURE

Bhabendra K. Pradhan, Avetik R. Harutyunyan and Peter C. Eklund*

[1]Department of Physics, The Pennsylvania State University, University Park, PA16802, USA

ABSTRACT

We report (6 wt %) storage of H_2 at T=77 K in processed bundles of single-walled carbon nanotubes at P=2 atmospheres. The hydrogen storage isotherms are completely reversible. D_2 isotherms confirm this anomalous low-pressure adsorption and further reveal the effects of quantum mechanical zero point motion. We propose that our post-synthesis treatment of the sample not only improves access for hydrogen to the central pores within individual nanotubes, but also may create a roughened tube surface with an enhanced binding energy for hydrogen. Such an enhancement is needed to understand the strong adsorption at low pressure. We obtain an experimental isosteric heat q_{st}=125 ± 5 meV for processed SWNT materials. We also studied H_2 adsorption in SWNTs produced by the High Pressure Carbonyl (HiPCo) process. We found up to ~2.5 wt% H_2 adsorbed on purified HIPCo material at 77K. The experimental isosteric heat for hydrogen storage in this material was found to be 76 ± 5 meV**.** High surface area activated carbon (SSA~ 1500 to 3200 m^2/g) were found to exhibit a reasonably high hydrogen sorption values (~4 to 5 wt %) at 77 K and pressure 16 bar.

INTRODUCTION

The ever-growing demand for energy, mediated by the 1990 Clean Air Act and 1992 Energy Policy Act in the United States has pointed out the need for the developments of cleaner fuels and more efficient engines [1]. Because of a limited supply and adverse environmental problems, fossil fuels must be replaced with pollution-free fuels derived from renewable resources. For these reason, Hydrogen is an ideal candidate providing more energy than fossil fuel on a weight basis. Hydrogen storage in a light weight carbon material would therefore be particularly attractive. The physical adsorption of gases within the micropores (diameter < nm) of carbon materials has been actively studied for more than 50 years [2]. Many such carbon materials have been developed with very high experimental specific surface areas of A_s ~ 1000 to 3000 m^2/g [3]. These materials tend to be disordered, with convoluted surfaces and predominately sp^2 C-C bonding. Despite these impressively large surface areas, these materials have not shown promise for hydrogen storage [2,3]. Recently reports of very high, reversible adsorption of molecular hydrogen in nano-carbon materials, i.e., pure carbon nanotubes, alkali-doped graphites, and pure and alkali-doped graphite nanofibers (GNFs) have generated tremendous interest in the research community, stimulating much experimental works and many theoretical studies worldwide[4-9]. In this study, we show that the wt% hydrogen adsorption depends on the post-synthesis treatment of the materials. SWNTs were carefully characterized with HRTEM, Raman scattering, N_2 adsorption isotherms.

*email: bkp5@psu.edu

EXPERIMENTAL

The SWNTs materials (arc-discharge derived: Ni-Y catalyzed) were obtained from Carbolex. This raw material was processed to remove amorphous and multi-shell carbon and residual catalyst. To accomplish this, the materials were first subjected to a high temperature oxidation under flow of dry air, then refluxed with mild mineral acid (HCl) in order to remove the exposed catalyst particles. The details of the purification is described elsewhere[10]. These samples were characterized by TEM, TPO, Raman scattering and N_2 adsorption isotherms. Transmission electron micrographs were observed on a JEOL JEM 1200EX microscope with electron beam energy of 120 kV. Raman spectra of the SWNTs samples were recorded in the Brewster-angle back scattering geometry for the following laser excitation lines: argon 514 nm (2.41 eV); krypton 647 nm (1.92 eV) and Nd:YAG 1064 nm (1.17 eV). Temperature programmed oxidation (TPO) of the samples were carried in gravimetric analyzer IGA-003 (Hiden Analytical Instruments). N_2 adsorption isotherms were measured at 77K using gravimetric analyzer IGA-003 (Hiden Analytical Instruments), prior to the adsorption, the sample was degassed under high vacuum (10^{-7} torr) at 500 K for overnight. The specific surface area and pores size were calculated by using BET and DR equations. Hydrogen uptake/storage measurements also carried out by using the same gravimetric sorption analyzer at 77K, which operate from UHV to 20 bar pressure range. An ultra high purity H_2 was used for the hydrogen uptake study using a oxygen/moisture trap on the delivery line. Prior to the hydrogen adsorption, the sample was degassed under high vacuum (10^{-8} torr) at 500-1223K for 12 h. Equilibrium at any pressure was achieved in less than 20 min, for each pressure point the time limit was set to be 30 min. In order to measure isosteric heat, we also measured hydrogen isotherm at 87 K. Most of the experiments were replicated to determine the reproducibility of the adsorption and desorption isotherms

RESULTS AND DISCUSSION

In Fig. 1a-d**,** we display high-resolution transmission electron microscopy (HRTEM) images for a sample of SWNT as-received (1a), and at successive processing steps (1b-d). For the as-received material, HRTEM images show primarily bundles of nanotubes and carbon-coated Ni-Y catalyst particles. To remove undesirable amorphous carbon that coats the SWNT bundles, we first selectively oxidized the amorphous carbon at T~350 °C in flowing dry air for 30 minutes. This oxidation also weakens the ordered sp^2 carbon coating passivating most of the metal catalyst particles in the soot, so that to 75 % to 90 % of the metal can be removed via a reflux in a mild mineral acid, i.e., 4.0 M HCl at T=130 °C for 18 h. On the basis of Raman scattering spectra and HRTEM images, it appears that HCl does not react with SWNT, but that HNO_3 does. This is important because the storage performance of the carbon sample is based on wt% uptake of hydrogen. Since our hydrogen storage experiments are conducted at room temperature and below, any metal in the sample can only decrease the wt% storage, as the metal cannot store (as hydride) at these temperatures.

A typical HRTEM image after a selective oxidation/HCl treatment (Fig. 1b) shows significant reduction in the catalyst residue (Ni-Y) content (to ~1.5 at % metal). The amorphous carbon that coats the bundle exterior has also been largely removed. A second sample was selectively oxidized, and then exposed to a considerably more aggressive oxidation in refluxing 2.6 M HNO_3

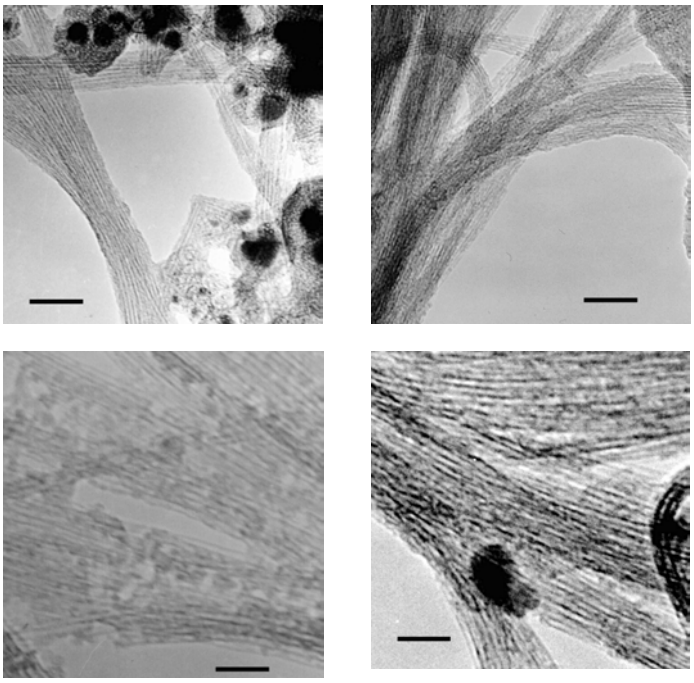

Fig. 1a-d. Transmission electron microscopy images of bundles of arc-derived carbon nanotubes at various stages of post synthesis processing: (a) as-received, (b) after selective oxidation/mild HCl reflux, (c) after selective oxidation followed by aggressive HNO_3 reflux, and (d) after step (c) followed by a heat treatment at 1000 °C in vacuum. Scale bar for (a) and (b) is 20 nm and for (c) and (d) is 10 nm.

at T=130 °C for 28 h. Although HNO_3 reflux removed almost all of the residual catalyst from the SWNT materials (i.e., less than 0.2 at % metal remained), significant damage to the tube wall (holes) can be seen in the HRTEM image (Fig. 1c). This extensive wall damage can be largely reversed by heating the material to 1000 °C in a high vacuum (P ~ 10^{-8} Torr) (Fig. 1d), as was reported earlier [14]. The apparent damage in our sample is considerably higher than reported previously. We also examined samples for H_2 storage that had received this HNO_3 reflux, and that were then vacuum annealed at low T (~300 °C, 12 hrs) or high T (1000 °C: 20hrs). Most of the functional groups attached to the tube ends and at wall defects, are expected to be desorbed in this 1000 °C vacuum treatment [14]. During 1000 °C anneals in our TGA apparatus, we observed sample weight losses in the range 5-45%, depending on the sample and its chemical treatment.

Figure 2 a-d also show Raman scattering spectra of these four sets of sample, taken at room temperature in the range 100 to 1700 cm^{-1}. Raman scattering is a sensitive probe of the structure and bonding in carbon materials, particularly, carbon nanotubes [12-13]. The spectra were excited with 1064 nm (Nd:Yag) laser radiation, which excites only the semi-conducting tubes via resonant Raman scattering [12]. The dominant spectral features include the low frequency radial breathing modes in the range ~150 to 200 cm^{-1} and the higher frequency tangential displacement modes in the range 1500 to 1600 cm^{-1} (Fig. 1a). The Raman-active radial breathing mode is the clear spectroscopic signature of the cylindrical seamless SWNT, and the diameter dependence of the mode frequency for tubes in the range 1.0 <d<1.4 nm is known to be approximately ω_R= (224 cm^{-1}. nm)/d(nm) ± Δ, where Δ~12 cm^{-1} corrects for the tube-tube interaction within a bundle [12]. The radial mode frequency and line-width are particularly sensitive to C-atom disorder
in the tube wall, and also to changes in the tube "bundling" brought about by post-synthesis treatment.

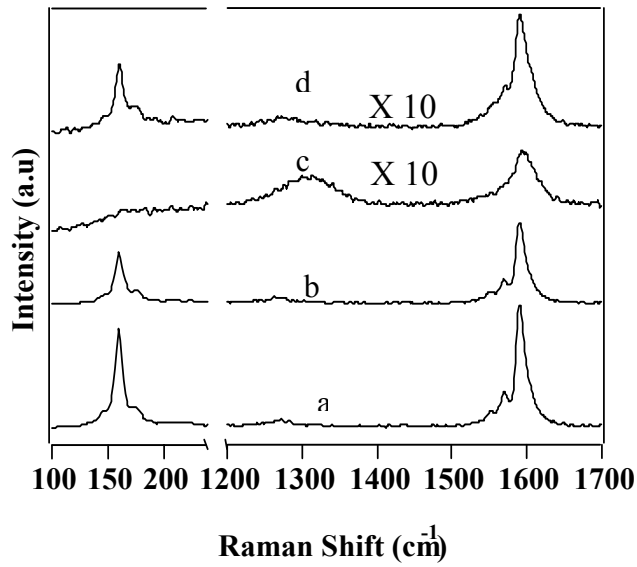

Fig. 2a-d. Room temperature Raman spectra of bundles of arc-derived carbon nanotubes at various stages of post synthesis processing: (a) as-received, (b) after selective oxidation/mild HCl reflux, (c) after selective oxidation followed by aggressive HNO_3 reflux, and (d) after step (c) followed by a heat treatment at 1000 °C in vacuum. The Raman spectra were taken using 1064 nm excitation.

The spectrum shown in Fig. 2a is typical of arc-derived material using a Ni-Y catalyst. In the as-delivered material the broad band centered near ~ 1300 cm^{-1} is weak relative to the band at ~ 1600 cm^{-1} (Fig.2a). This band (at 1350 cm^{-1}), commonly called the D-band, has been observed in many sp^2-bonded carbon materials and is associated with disorder(D) in the hexagonal carbon network. In the case of a multi-carbon phase SWNT material, the D-band could be identified either with amorphous sp^2 carbon present in nanoparticles, or in a thin coating on the nanotube bundle exterior. However, a D-band can also arise from disorder within the hexagonal carbon network of the nanotube wall itself. The fact that spectrum (a) has a weak D-band indicates that the sample contains a small amount of amorphous carbon and that the nanotube walls have a low number of defects. Chemical processing (particularly, in case of HNO_3), as shown below, was found to have a dramatic effect on the disorder in the system as seen via the D-band whose intensity correlates with the degree of disorder in the sp^2 network. Comparing the spectrum of Fig. 2a to that of Fig. 2b, we see that selective oxidation (Table 1), followed by HCl reflux, has no significant effect on the Raman spectrum of the as-prepared material. This was verified by a careful Lorentzian lineshape analysis, by comparison, for the full width at half maximum (FWHM) of the T Raman bands. No change in the FWHM following selective oxidation and HCl reflux was observed.

However, refluxing in the much more aggressive HNO_3 for 28 hrs alters the Raman spectrum dramatically (Fig. 2c): the D-band at ~1350 cm^{-1} is much stronger; the tangential band (or G band) broadens significantly; and the radial band broadens to the point of near invisibility. The HNO_3 reflux has clearly damaged the SWNT, consistent with the TEM images. However, after this treatment we heat the sample in situ under vacuum to ~250 °C. This temperature should be sufficient to remove any residual HNO3 as NO_x, so the intercalation compound has been essentially destroyed. The functionalization of the tube wall has occurred and does give rise to increased Raman line widths and to an increase in the D band intensity. This is the case because these functional groups do in fact induced disorder on the tube wall. However, it is important to consider the likely wall sites where these functional groups would attach themselves. These sites are at near missing C-atom sites in the tube walls, i.e., on the edges of holes in the tube wall. The disappearance of the radial band can be caused by the disorder in the tube wall via functional groups at the damage sites caused by the acid treatment. This explanation is associated with a softening and broadening of the Raman-active radial mode anticipated from the wall damage/functionalization. It was surprising to us that the final high-T anneal at 1000 °C (~20 hrs) almost completely restores the Raman spectrum (Fig 2d) to that of the as-prepared (starting) material: The D-band is significantly reduced in intensity; the tangential bands have narrowed considerably; and the radial band regathers strength. The restoration of structural order to the SWNT is remarkable. Apparently, SWNTs can heal at significantly lower temperatures than needed for graphitization (T > 2000 °C). However, a careful line-shape analysis of the Raman bands after the vacuum anneal reveals that a residual line broadening associated with remnant disorder in the SWNT wall does indeed exist. A pervasive reminant disorder could enhance the binding energy of H_2 as discussed below.

The post-synthesis processing for each sample is summarized in Table 1, together with the at% metal residue and specific surface area (SSA) (m^2/g). The vacuum heat-treatment and the SSA measurements were made *in situ* in the TGA just prior to H_2 loading. The SSA values (250-470 m^2/g) are quite low compared to the maximum geometric surface area of a large bundle of open SWNTs ~1350 m^2/g. Furthermore, we find that the SSA does not correlate

Table 1. Sample history and hydrogen storage at 77 K and 1 atmosphere.

Sample	Sample History	SSA[4] (m	Vac. Ann T(°C)/time (	Metal %)[5]
A	SWNTs	270	250/12	6
B	SO[1], HCl[2]	470	1000/20	1.5
C	SO[1], HNO3[3]	250	1000/20	<0.2

[1] (SO) Selective Oxidation at 350 °C for 30-45 min in flowing air (100 CCM).
[2] Reflux in 4M HCl at 120 °C for 6 hr.
[3] Reflux in 2.6 M HNO_3 at 130 °C for 30 hr.
[4] Specific Surface Area (BET) [15].
[5] Determined by Temp. Prog. Oxid. (TPO).

with wt% H_2 storage. Although the theoretical SSA associated with the internal pore surface of a ~1.4 nm diameter SWNT is ~1350 m^2/g, no one has yet reported values exceeding~400 m^2/g for SWNT materials. This indicates that the N_2 molecule is too large to gain access to many of these internal pores in a real material, we conclude that the gateways must be smaller that the kinetic diameter of N_2 ~ 0.36 nm [15]. As pointed out previously [14], this restricted gateway may be associated with the presence of carboxylic acid and other functional groups attached to carbon atoms present around holes in the tube walls or at open tube ends. The real gateways to the internal pore of the SWNT are, in many cases, apparently small enough to block entry of N_2, but not H_2.

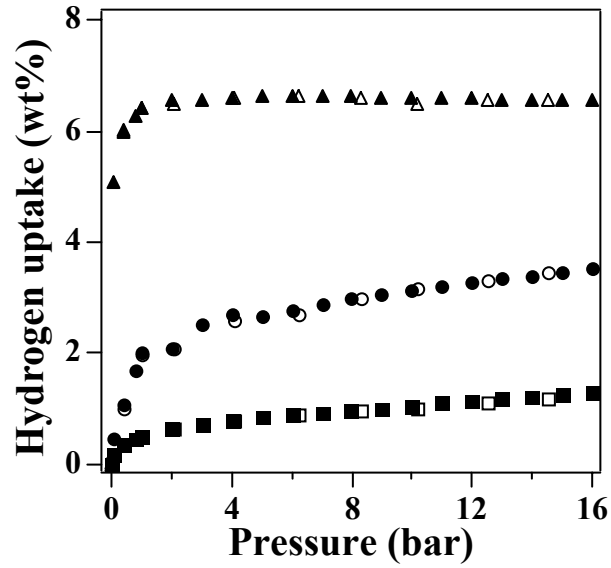

Fig. 3. Hydrogen isotherms (T=77 K) showing progressively better wt% H_2 storage with nanotube processing. From bottom to top, (a)the isotherms were taken on as-received material, (b). after selective oxidation/mild HCl reflux, followed by a heat treatment at 1000 C in vacuum (10^{-7} torr) for 20 hrs and (c) after selective oxidation/mild HNO_3 reflux, followed by a heat treatment at 1000 C in vacuum (10^{-7} torr) for 20 hrs.

In Fig. 3, we show low temperature isotherms for three samples labeled A, B and C (detail sample description in Table 1). The most remarkable feature of the H_2 storage isotherms of Fig. 3 is the very low H_2 overpressure required for significant storage in the processed SWNT material. Furthermore, the open symbols in the figure refer to adsorption, and the closed to desorption data. As can be seen in the figure, the adsorption/desorption data are completely retraceable. This rules out the adsorption at 77 K of gases such as H_2O and O_2. We can compare our data for the HNO_3 treated material to that of Ye et al [8] who reported a maximum of ~ 8 wt% storage at T=77 and ~100 atm. Their H_2 over-pressures are a factor of 20 - 40 higher than required in our material to achieve similar storage. This remarkable change in the pressure scale suggests to us that the disorder we have created in the individual SWNT and bundling thereof may play an important role in enhancing the binding energy for H_2 adsorption.

Figure 4. compares the T=77 K isotherms for hydrogen and deuterium (D_2) on the same sample. Data were first collected with H_2. Next the sample was degassed in vacuum at 250 °C for 12 hr and cooled to 77 K to collect the D_2 isotherm. The wt% storage for D_2 confirms the high storage observed for H_2 at low pressure in the same sample. It also reveals the effect of the quantum mechanical zero point motion on the storage. That is, since the

observed wt% (D_2) is more than twice the wt% (H_2), the storage is larger than the simple enhancement stemming from the larger isotopic mass of D_2. The enhancement in the surface binding energy of deuterium over hydrogen is approximately 1/2 the mean kinetic energy of vibration (<KE>) of the molecule in the pore. <KE> depends on the nature of the confinement of the molecule in the pore (e.g., interstitial channels in the bundle, internal pore of an individual nanotube), and thus the size of the isotope effect can give indirect information on pore volume and shape.

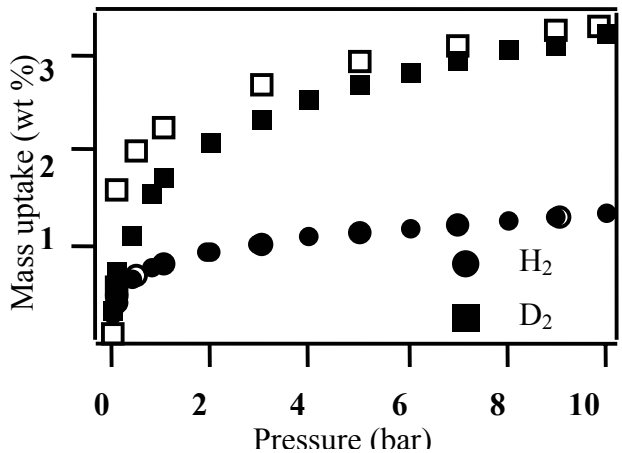

Figure 4. H_2 and D_2 adsorption isotherms on purified SWNTs at 77K, close symbols for adsorption and open symbol for desorption respectively.

The Isosteric heat of adsorption, q_{st}=Rd(lnP)/d(1/T), depends upon the binding energy of the molecule to the surface; R is the gas constant and P is the pressure [15]. We can estimate q_{st} using data from two isotherms collected at T=77 and 87 K. For our highest storage sample (C), we find the isosteric heat to be 125±5 meV. The isosteric heat bears a simple relation to the binding energy only within certain models or regimes of behavior. For example, a low density gas on a planar surface obeys $q_{st} = \langle E_z \rangle + (3/2)$ kT, where $\langle E_z \rangle$ is the mean binding energy of surface-normal motion, computed quantum-mechanically. At T=77 K, kT ~ 6 meV, so in our case, we expect that the isosteric heat and the binding energy are nearly equal, independent of the details of the confinement. The magnitude of q_{st} substantially exceeds that expected for adsorption of H_2 to a planar sheet of graphite. This observation motivates a consideration of geometry-specific mechanisms for enhancing adsorption.

The end result of the aggressive HNO_3 treatment is a heavily damaged tube covered with holes of various sizes. This defective structure is far from equilibrium; the system can gain stability by partial healing the holes during the post-treatment anneal. The resulting tubes have irregular shapes and roughened surfaces. Atom transport during the healing must, of geometric necessity, produce pentagonal and heptagonal carbon rings. Pentagonal rings are particularly favored, as they most efficiently cap bonds on edge atoms bordering the holes. Such irregularities might open the small interstitial channels of pristine bundles into wider interstitial galleries, if the surface energy at the inter-tube contact does not dominate atomic rearrangement during annealing.

CONCLUSIONS

These results suggest an intimate connection between structural metastability and enhanced adsorption. A substrate near its global structural ground state has found a very efficient means to self-bind. If some component of the substrate-substrate interactions mimics the substrate-adsorbate interaction (e.g. graphene sheets bind to each other with an interaction mechanism not far removed from that of substrate-adsorbate physisorption), then a nearly-equilibrium self-bound structure will not be optimized for highest adsorption. Instead, a larger adsorption energy may occur in structures wherein the carbon substrate is unable to fully accrue the energetic advantages of self-binding. Our calculations suggest that the aggressive HNO_3 treatment pushes the material far from structural equilibrium by creating large holes in the tube walls. Partial healing during the subsequent anneal then spreads this disequilibrium more evenly throughout the structure and could yield a substrate with enhanced physisorption at low pressure, if the roughening is sufficiently pervasive.

REFERENCES

1. G.D. Berry, S. M. Aceves, Energy &Fuels, 12, 49, 1998.
2. S. Hynek, W. Fuller and J. Bentley, Int. J. Hydrogen Energy, 22, 601, 1997.
3. R. K. Agarwal, J. S. Noh, J. A. Schwarz and P. davini, Carbon, 25, 219, 1987.
4. A. C. Dillon, K. M. Jones, T.A. Bekkedahl, C. H. Kiang, D. S. Bethune, and M. J. Heben, *Nature* 386, 377-379 (1997).
5. C. Liu, Y. Y. Fan, M. Liu, H. T. Cong, H. M. Cheng, and M. S. Dresselhaus, *Science*, 286, 1127-1129 (1999).
6. P. Chen, X. Wu, J. Lin, and K. L. Tan, *Science*, 285, 91--93 (1999).
7. A. Chambers, C. Park, R. T. K. Baker, and N. M. Rodriguez, *J. Phys. Chem., B* 102, 4253-4256 (1998).
8. Y. Ye, C. C. Ahn, C. Witham, B. Fultz, J. Liu, A. G. Rinzler, D. Colbert, K. A. Smith, and R. E. Smalley, *Appl. Phys. Lett.* 74, 2307--2309 (1999).
9. M.S. Dresselhaus, K. A. Williams, and P. C. Eklund, MRS Bull, 45, 1999
10. B.K.Pradhan, A.R.Harutyunyan, P.C.Eklund, PSU Invention Disclosure No.2001-2445, 2001
11. CarboLex Inc; web site: www.carbolex.com.
12. M.S. Dresselhaus and P. C. Eklund, *Adv. In Phys*. **49**, 705 (2000).
13. M.S. Dresselhaus, G. Dresselhaus, P. C. Eklund, *Science of Fullerenes and Carbon Nanotubes*, (Academic Press, San Diego, 1996).
14. D. B. Mawhinney etal Chem. Phys. Lett., 324, 213, 2000.
15. S. J. Gregg and K. S. W. Sing, Adsorption, Surfacce Area and Porosity, (Academic Press, 1982).

Acknowledgements: This work was supported by Honda R&D JAPAN.